

# Entanglement between deconfinement transition and chiral symmetry restoration

Yuji Sakai,<sup>1,\*</sup> Takahiro Sasaki,<sup>1,†</sup> Hiroaki Kouno,<sup>2,‡</sup> and Masanobu Yahiro<sup>1,§</sup>

<sup>1</sup>*Department of Physics, Graduate School of Sciences, Kyushu University, Fukuoka 812-8581, Japan*

<sup>2</sup>*Department of Physics, Saga University, Saga 840-8502, Japan*

(Dated: November 17, 2018)

We extend the Polyakov-loop extended Nambu–Jona-Lasinio (PNJL) model by introducing an effective four-quark vertex depending on Polyakov loop. The effective vertex generates entanglement interactions between Polyakov loop and chiral condensate. The new model is consistent with lattice QCD data at imaginary quark-number chemical potential and real and imaginary isospin chemical potentials, particularly on strong correlation between the chiral and deconfinement transitions and also on the quark-mass dependence of the order of the Roberge-Weiss endpoint. We investigate the influence of the entanglement interactions on the location of the tricritical point at real isospin chemical potential and on the location of the critical endpoint at real quark-number chemical potential.

PACS numbers: 11.30.Rd, 12.40.-y

## I. INTRODUCTION

An important query on the thermodynamics of quantum chromodynamics (QCD) is whether the chiral-symmetry restoration and the confinement-to-deconfinement transition take place simultaneously or not. If the two transitions do not coincide, phases such as the constituent quark phase [1, 2] or the quarkyonic phase [3, 4] may appear.

If the chiral and deconfinement transitions are of first order, discontinuities appear simultaneously in their (approximate) order parameters, that is, the chiral condensate  $\sigma$  and the Polyakov loop  $\Phi$  [5, 6]. Furthermore, if a nontrivial critical endpoint (CEP) exists at finite temperature ( $T$ ) and quark-number chemical potential  $\mu_q$  [7], susceptibilities of  $\sigma$ ,  $\Phi$  and other quantities diverge simultaneously [8]. This indicates a coincidence of second-order phase transitions. At zero  $\mu_q$ , the chiral and deconfinement transitions are found to be crossover [9]. Hence, there is no a priori reason why the two transitions coincide exactly. Actually, in lattice QCD (LQCD) simulations at zero chemical potential [9–11], there is a debate as to whether the transitions really coincide or not; see Ref. [12] and references therein. LQCD simulations are far from perfection at real  $\mu_q$  because of the well-known sign problem [13]. Fortunately, LQCD data are available at imaginary  $\mu_q$  [14–22] and real and imaginary isospin chemical potential  $\mu_I$  [23–25], since LQCD has no sign problem there. The data show that chiral and deconfinement crossover transitions coincide within the numerical accuracy. Since there is no general reason for exact coincidence between crossover transitions, it is natural to think that the chiral and deconfinement crossover transitions nearly coincide as a result of strong correlation (entanglement) between  $\sigma$  and  $\Phi$ . We investigate this possibility in the present paper.

As an approach complementary to first-principle LQCD,

we can consider effective models such as the Nambu–Jona-Lasinio (NJL) model [7, 8, 26–30] and the Polyakov-loop extended Nambu–Jona-Lasinio (PNJL) model [6, 31–54]. The NJL model can describe chiral symmetry breaking, but not the confinement mechanism. The PNJL model is designed [33] to make it possible to treat both the mechanisms. The PNJL model can reproduce results of LQCD at zero and imaginary  $\mu_q$  [47–50] where LQCD has no sign problem.

At imaginary  $\mu_q = i\theta_q T$ , the grand canonical partition function  $Z_{GC}(\theta_q)$  of QCD is related to the thermodynamic potential  $\Omega_{QCD}$  as  $\Omega_{QCD}(\theta_q) = -T \ln(Z_{GC}(\theta_q))$ , where  $\theta_q$  is a real parameter. Roberge and Weiss (RW) found [55] that QCD has a periodicity  $\Omega_{QCD}(\theta_q) = \Omega_{QCD}(\theta_q + 2\pi k/3)$ , showing that  $\Omega_{QCD}(\theta_q + 2\pi k/3)$  is transformed into  $\Omega_{QCD}(\theta_q)$  by the  $\mathbb{Z}_3$  transformation with integer  $k$ . This means that QCD is invariant under a combination of the  $\mathbb{Z}_3$  transformation and a parameter transformation  $\theta_q \rightarrow \theta_q + 2k\pi/3$  [47, 48],

$$\begin{aligned} q &\rightarrow Uq, & A_\nu &\rightarrow UA_\nu U^{-1} - i/g(\partial_\nu U)U^{-1}, \\ \theta_q &\rightarrow \theta_q + 2\pi k/3, \end{aligned} \quad (1)$$

where  $U(x, \tau)$  are elements of SU(3) with  $U(x, \beta = 1/T) = \exp(-2i\pi k/3)U(x, 0)$ ,  $q$  is the quark field and  $A_\nu$  is the gauge field. We call this combination extended  $\mathbb{Z}_3$  transformation. Thus,  $\Omega_{QCD}(\theta_q)$  has the extended  $\mathbb{Z}_3$  symmetry, and hence quantities invariant under the extended  $\mathbb{Z}_3$  transformation have RW periodicity [47, 48]. At the present stage, the PNJL model is only a realistic effective model that possesses both extended  $\mathbb{Z}_3$  symmetry and chiral symmetry [47, 48]. Furthermore, the PNJL model can reproduce the first-order RW transition [55] that occurs at  $\theta_q = (2k+1)\pi/3$  when  $T$  is larger than some critical temperature  $T_E$ . This property makes it possible to compare PNJL results with LQCD data quantitatively at imaginary  $\mu_q$ . A current topic at imaginary  $\mu_q$  is what the order of the RW transition is at the endpoint  $T = T_E$ . The recent LQCD simulations show that it is first-order for small and larger quark masses, but the order is weakened and could be second order at intermediate masses [19, 20].

In the PNJL model, the correlation between  $\sigma$  and  $\Phi$  is weak, so that the chiral and deconfinement crossover transitions do not coincide without any fine-tuning of param-

\*sakai@phys.kyushu-u.ac.jp

†sasaki@phys.kyushu-u.ac.jp

‡kounoh@cc.saga-u.ac.jp

§yahiro@phys.kyushu-u.ac.jp

ters [49]. For zero chemical potential, the scalar-type eight-quark interaction is necessary to obtain a coincidence between the two transitions, and for imaginary  $\mu_q$  the vector-type four-quark interaction is needed [49]. This fact indicates that a true correlation between  $\sigma$  and  $\Phi$  is stronger than that in the PNJL model appearing through the covariant derivative between quark and gauge fields. Actually, recent analyses [56, 57] based on the exact renormalization-group (ERG) equation [58] indicate that entanglement interactions between  $\sigma$  and  $\Phi$  appear in addition to the original entanglement through the covariant derivative.

In this paper, we extend the PNJL model by introducing an effective four-quark vertex depending phenomenologically on  $\Phi$ . The effective vertex generates entanglement interactions between  $\sigma$  and  $\Phi$ . The functional form of the entanglement vertex is determined by respecting the extended  $\mathbb{Z}_3$  symmetry and the chiral symmetry. The strength of the vertex is determined from LQCD data at imaginary  $\mu_q$ , and the validity of the model setting is confirmed for real and imaginary values of  $\mu_I$  by comparing the model results with LQCD data. The new model is consistent with all LQCD data at imaginary  $\mu_q$  and real and imaginary  $\mu_I$ . Particularly, the new model can reproduce two phenomena simultaneously; one is the strong correlation between the deconfinement and chiral transitions and the other is the quark-mass dependence of the RW endpoint predicted by LQCD very recently [19, 20]. We also analyze the influence of the entanglement interactions on the location of the tricritical point (TCP) in  $\mu_I$ - $T$  plane and the location of the critical endpoint (CEP) in  $\mu_q$ - $T$  plane. The present phenomenological approach is complementary to the ERG approach mentioned above.

In Sec. II, we explain the PNJL model briefly and introduce an effective four-quark vertex depending on  $\Phi$ . In Sec. III, the new model with the effective vertex is applied to the imaginary  $\mu_q$  region and the real and imaginary  $\mu_I$  regions and compared with LQCD there. Sec. IV is devoted to a summary.

## II. PNJL MODEL

We start with the standard two-flavor PNJL Lagrangian [33, 35]

$$\mathcal{L} = \bar{q}(i\gamma_\nu D^\nu - m_0)q + G_s[(\bar{q}q)^2 + (\bar{q}i\gamma_5\vec{\tau}q)^2] - \mathcal{U}[\Phi[A], \Phi[A]^*, T], \quad (2)$$

where  $q$  denotes the two-flavor quark field,  $m_0$  denotes the current quark mass, and  $D^\nu = \partial^\nu + iA^\nu - i\mu_q\delta_0^\nu$ . Field  $A^\nu$  is defined as  $A^\nu = \delta_0^\nu g A_a^0 \frac{\lambda_a}{2}$ , with gauge fields  $A_a^\nu$ , the Gell-Mann matrix  $\lambda_a$ , and the gauge coupling  $g$ . In the NJL sector,  $G_s$  denotes the coupling constant of the scalar-type four-quark interaction. The Polyakov potential  $\mathcal{U}$ , defined in (7), is a function of Polyakov loop  $\Phi$  and its Hermitian conjugate  $\Phi^*$ ,

$$\Phi = \frac{1}{N_c} \text{Tr} L, \quad \Phi^* = \frac{1}{N_c} \text{Tr} L^\dagger, \quad (3)$$

with

$$L(\mathbf{x}) = \mathcal{P} \exp \left[ i \int_0^\beta d\tau A_4(\mathbf{x}, \tau) \right], \quad (4)$$

where  $\mathcal{P}$  is the path ordering and  $A_4 = iA_0$ . In the chiral limit ( $m_0 = 0$ ), the Lagrangian density has the exact  $SU(N_f)_L \times SU(N_f)_R \times U(1)_v \times SU(3)_c$  symmetry. The temporal component of the gauge field is diagonal in flavor space, because color and flavor spaces are completely separated in the present case. In the Polyakov gauge,  $L$  can be written in a diagonal form in color space [33]:

$$L = e^{i\beta(\phi_3\lambda_3 + \phi_8\lambda_8)} = \text{diag}(e^{i\beta\phi_a}, e^{i\beta\phi_b}, e^{i\beta\phi_c}), \quad (5)$$

where  $\phi_a = \phi_3 + \phi_8/\sqrt{3}$ ,  $\phi_b = -\phi_3 + \phi_8/\sqrt{3}$  and  $\phi_c = -(\phi_a + \phi_b) = -2\phi_8/\sqrt{3}$ . The Polyakov loop  $\Phi$  is an exact order parameter of spontaneous  $\mathbb{Z}_3$  symmetry breaking in pure gauge theory. Although  $\mathbb{Z}_3$  symmetry is not an exact one in the system with dynamical quarks, it still seems to be a good indicator of the deconfinement phase transition. Therefore, we use  $\Phi$  to define the deconfinement phase transition.

Making the mean field approximation and performing the path integral over the quark field, one can obtain the thermodynamic potential  $\Omega$  (per volume),

$$\begin{aligned} \Omega = & -2N_f \int \frac{d^3\mathbf{p}}{(2\pi)^3} \left[ 3E(\mathbf{p}) \right. \\ & + \frac{1}{\beta} \ln [1 + 3(\Phi + \Phi^* e^{-\beta E^-(\mathbf{p})}) e^{-\beta E^-(\mathbf{p})} + e^{-3\beta E^-(\mathbf{p})}] \\ & + \frac{1}{\beta} \ln [1 + 3(\Phi^* + \Phi e^{-\beta E^+(\mathbf{p})}) e^{-\beta E^+(\mathbf{p})} + e^{-3\beta E^+(\mathbf{p})}] \\ & \left. + U_M + \mathcal{U}, \right] \quad (6) \end{aligned}$$

where  $\sigma = \langle \bar{q}q \rangle$ ,  $\Sigma_s = -2G_s\sigma$ ,  $M = m_0 + \Sigma_s$ ,  $U_M = G_s\sigma^2$ ,  $E(\mathbf{p}) = \sqrt{\mathbf{p}^2 + M^2}$  and  $E^\pm(\mathbf{p}) = E(\mathbf{p}) \pm \mu_q = E(\mathbf{p}) \pm i\theta_q/\beta$ . On the right-hand side of (6), only the first term diverges. It is then regularized by the three-dimensional momentum cutoff  $\Lambda$  [33–35]. We use  $\mathcal{U}$  of Ref. [38], which is fitted to a LQCD simulation in pure gauge theory at finite  $T$  [59, 60]:

$$\begin{aligned} \mathcal{U} = & T^4 \left[ -\frac{a(T)}{2} \Phi^* \Phi \right. \\ & \left. + b(T) \ln(1 - 6\Phi\Phi^* + 4(\Phi^3 + \Phi^{*3}) - 3(\Phi\Phi^*)^2) \right] \quad (7) \end{aligned}$$

with

$$a(T) = a_0 + a_1 \left( \frac{T_0}{T} \right) + a_2 \left( \frac{T_0}{T} \right)^2, \quad b(T) = b_3 \left( \frac{T_0}{T} \right)^3, \quad (8)$$

where the parameters are summarized in Table I. In pure gauge theory, the Polyakov potential yields a first-order deconfinement phase transition at  $T = T_0$ . It is determined from pure gauge LQCD that  $T_0 = 270$  MeV. In QCD with two-flavor dynamical quarks at  $\mu_q = 0$ , the PNJL model with the original value of  $T_0$  shows that the pseudocritical

temperatures of chiral and deconfinement crossover transitions are  $T_\sigma \approx 230$  MeV and  $T_\Phi \approx 215$  MeV, respectively [35], while full LQCD simulations [9, 61, 62] show that  $T_\sigma \approx T_\Phi \approx 173 \pm 8$  MeV. It follows from these results that the relative difference  $\Delta = |T_\sigma - T_\Phi|/T_\sigma$  is about 6% for the PNJL model and at most 10% for LQCD. Thus, for  $\Delta$  the PNJL result is consistent with the LQCD data, but for the absolute values of  $T_\sigma$  and  $T_\Phi$  the PNJL result is larger than the LQCD data. Therefore, we rescale  $T_0$  to 212 MeV in the PNJL model to obtain  $T_\Phi = 173$  MeV. However, the PNJL calculation with the four-quark interaction only shows that  $T_\sigma = 216$  MeV and  $\Delta \approx 20\%$  [49]. The results on  $T_\sigma$  and  $\Delta$  are not consistent with the LQCD results. This indicates that the entanglement between the chiral and deconfinement transitions is weak in the PNJL model. This problem will be discussed later and solved in this paper.

$a_0$	$a_1$	$a_2$	$b_3$
3.51	-2.47	15.2	-1.75

TABLE I: Summary of the parameter set in the Polyakov sector used in Ref. [38]. All parameters are dimensionless.

The variables  $X = \Phi$ ,  $\Phi^*$  and  $\sigma$  satisfy the stationary conditions

$$\partial\Omega/\partial X = 0. \quad (9)$$

The solutions of the stationary conditions do not necessarily yield a global minimum  $\Omega$ . There is a possibility that they yield a local minimum or even a maximum. We then checked that the solutions yield a global minimum when the solutions  $X(\theta_q)$  are inserted back into (6).

The thermodynamic potential  $\Omega$  of (6) is not invariant under the  $\mathbb{Z}_3$  transformation,

$$\Phi(\theta_q) \rightarrow \Phi(\theta_q)e^{-i2\pi k/3}, \quad \Phi(\theta_q)^* \rightarrow \Phi(\theta_q)^*e^{i2\pi k/3}, \quad (10)$$

although  $\mathcal{U}$  of (7) is invariant. Instead of  $\mathbb{Z}_3$  symmetry, however,  $\Omega$  is invariant under the extended  $\mathbb{Z}_3$  transformation [47],

$$\begin{aligned} e^{\pm i\theta_q} &\rightarrow e^{\pm i\theta_q}e^{\pm i\frac{2\pi k}{3}}, & \Phi(\theta_q) &\rightarrow \Phi(\theta_q)e^{-i\frac{2\pi k}{3}}, \\ \Phi(\theta_q)^* &\rightarrow \Phi(\theta_q)^*e^{i\frac{2\pi k}{3}}. \end{aligned} \quad (11)$$

This is easily understood as follows. It is convenient to introduce the modified Polyakov loop  $\Psi \equiv e^{i\theta_q}\Phi$  and  $\Psi^* \equiv e^{-i\theta_q}\Phi^*$  invariant under the transformation (11). The extended  $\mathbb{Z}_3$  transformation is then rewritten as

$$\begin{aligned} e^{\pm i\theta_q} &\rightarrow e^{\pm i\theta_q}e^{\pm i\frac{2\pi k}{3}}, & \Psi(\theta_q) &\rightarrow \Psi(\theta_q), \\ \Psi(\theta_q)^* &\rightarrow \Psi(\theta_q)^*, \end{aligned} \quad (12)$$

and  $\Omega$  is rewritten as

$$\begin{aligned} \Omega = & -2N_f \int \frac{d^3\mathbf{p}}{(2\pi)^3} \left[ 3E(\mathbf{p}) + \frac{1}{\beta} \ln [1 + 3\Psi e^{-\beta E(\mathbf{p})}] \right. \\ & + 3\Psi^* e^{-2\beta E(\mathbf{p})} e^{\beta\mu_B} + e^{-3\beta E(\mathbf{p})} e^{\beta\mu_B} \\ & + \frac{1}{\beta} \ln [1 + 3\Psi^* e^{-\beta E(\mathbf{p})} + 3\Psi e^{-2\beta E(\mathbf{p})} e^{-\beta\mu_B} \\ & \left. + e^{-3\beta E(\mathbf{p})} e^{-\beta\mu_B}] \right] + U_M + \mathcal{U}, \end{aligned} \quad (13)$$

where  $\beta\mu_B = 3\beta\mu_q = 3i\theta_q$ . Obviously,  $\Omega$  is invariant under the extended  $\mathbb{Z}_3$  transformation (12), since it is a function of only extended  $\mathbb{Z}_3$  invariant quantities,  $e^{3i\theta_q}$  and  $\tilde{X} (= \Psi, \Psi^*, \sigma)$ . The explicit  $\theta_q$  dependence appears only through a factor  $e^{3i\theta_q}$  in (13). Hence, the stationary conditions (9) show that  $\tilde{X} = \tilde{X}(e^{3i\theta_q})$ . Inserting the solutions back to (13), one can see that  $\Omega = \Omega(e^{3i\theta_q})$ . Thus,  $\tilde{X}$  and  $\Omega$  have the RW periodicity,

$$\tilde{X}(\theta_q + \frac{2\pi k}{3}) = \tilde{X}(\theta_q), \quad \text{and} \quad \Omega(\theta_q + \frac{2\pi k}{3}) = \Omega(\theta_q), \quad (14)$$

while the Polyakov loop  $\Phi$  and its Hermitian conjugate  $\Phi^*$  have the properties

$$\begin{aligned} \Phi(\theta_q + \frac{2\pi k}{3}) &= e^{-i2\pi k/3}\Phi(\theta_q), \\ \Phi(\theta_q + \frac{2\pi k}{3})^* &= e^{i2\pi k/3}\Phi(\theta_q)^*. \end{aligned} \quad (15)$$

The RW periodicity is a remnant of  $\mathbb{Z}_3$  symmetry in the pure gauge limit. In QCD with dynamical quarks, there appear three  $\mathbb{Z}_3$  vacua, when  $T$  is larger than a critical temperature  $T_E$ . The  $\mathbb{Z}_3$  vacua are classified by the phase  $\phi$  of  $\Phi$ , and each has anyone of  $\phi$ ,  $\phi + 2\pi/3$  and  $\phi + 4\pi/3$ . Roberge and Weiss [55] found that there is a first-order phase transition at  $\theta_q = \pi/3 \bmod 2\pi/3$  where the ground state is changed from a vacuum to its  $\mathbb{Z}_3$  images; the RW phase transition is illustrated in Fig. 6 (shown later). The transition is called the "Roberge-Weiss transition." In this transition, charge conjugation (C) symmetry is spontaneously broken and  $\theta_q$ -odd quantities such as the phase  $\psi$  of  $\Psi$  are order parameters of the transition [50].

In the ordinary PNJL model with the scalar-type four-quark interaction only, the chiral transition occurs at higher  $T$  than the deconfinement transition, unlike LQCD data at zero and imaginary  $\mu_q$ . In Ref. [49], we revealed that the PNJL model with the scalar-type eight-quark interaction [29, 30, 47],

$$G_{s8}[(\bar{q}q)^2 + (\bar{q}i\gamma_5\vec{\tau}q)^2]^2, \quad (16)$$

and the vector-type four-quark interaction [28, 30, 48],

$$G_v(\bar{q}\gamma_\nu q)^2, \quad (17)$$

can reproduce LQCD data at imaginary  $\mu_q$ . Since the coupling constants,  $G_{s8}$  and  $G_v$ , of the interactions are adjusted to the LQCD data, the correlation between  $\sigma$  and  $\Phi$  is still weaker in this model than in LQCD. We then propose another possibility to explain the strong correlation shown in LQCD.

The origin of the four-quark vertex  $G_s$  is the one-gluon exchange diagram between two quarks and its higher-order diagrams. If the gluon field  $A_\nu$  has a vacuum expectation value  $\langle A_0 \rangle$  in its time component,  $A_\nu$  is coupled to  $\langle A_0 \rangle$  which is related to  $\Phi$  through (5) [57]; see Fig. 1 for the diagrammatic description. Hence,  $G_s$  is changed into an effective vertex  $G_s(\Phi)$  that can depend on  $\Phi$  [57]. The effective vertex  $G_s(\Phi)$  is called the entanglement vertex, and all interactions including  $G_s(\Phi)$  are referred to as the entanglement interactions. It is expected that the  $\Phi$  dependence of  $G_s(\Phi)$  will be determined in the future by an exact method such as ERG [56–58]. In this paper, however, we simply assume the following  $G_s(\Phi)$  that preserves chiral symmetry, C symmetry [32, 50] and extended  $\mathbb{Z}_3$  symmetry [47]:

$$G_s(\Phi) = G_s[1 - \alpha_1 \Phi \Phi^* - \alpha_2 (\Phi^3 + \Phi^{*3})]. \quad (18)$$

In the mean field approximation, the mesonic potential  $U_M$  is modified as follows,

$$U_M(\sigma, \Phi) = G_s[1 - \alpha_1 \Phi \Phi^* - \alpha_2 (\Phi^3 + \Phi^{*3})] \sigma^2 \quad (19)$$

and the constituent quark mass is changed into

$$M = m_0 - 2G_s(\Phi)\sigma. \quad (20)$$

Thus, this model has entanglement interactions between  $\sigma$  and  $\Phi$  in addition to the covariant derivative in the original PNJL model. The gap equation (9) can be evaluated by using the chain rules even in the presence of the entanglement interactions.

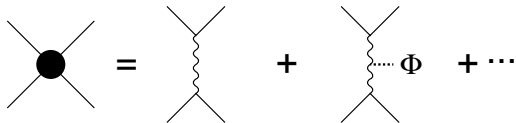


Fig. 1: The diagrammatic description of the effective vertex  $G_s(\Phi)$ .

In this paper, the original PNJL model is simply called PNJL. The PNJL model with the entanglement vertex  $G_s(\Phi)$  is referred to as entanglement PNJL (EPNJL), while the PNJL model with the scalar-type eight-quark and the vector-type four-quark interaction is referred to as PNJL-8V.

### III. NUMERICAL RESULTS

In this section, we consider the case of  $N_f = 2$ , and take  $m_0 = 5.5$  MeV unless otherwise mentioned. In the PNJL and PNJL-8V models, we take the same parameter set as in the previous analysis of Ref. [49]. In the EPNJL model, we take the same parameter set as the PNJL model, but  $T_0$  is taken to be 190 MeV so as to reproduce LQCD data at  $\mu_q = 0$ , when  $(\alpha_1, \alpha_2) = (0.2, 0.2)$ . This parameter set reproduces LQCD data at zero  $\mu_q$  on the coincidence between  $T_\sigma$  and  $T_\Phi$  [9, 61, 62] and at imaginary  $\mu_q$  on the  $m_0$  dependence of the order of the RW endpoint [19]. Qualitative properties

such as the coincidence and the  $m_0$  dependence are preserved in the parameter region  $\alpha_1, \alpha_2 \approx 0.20 \pm 0.05$ . The validity of the parameter set in the EPNJL model is confirmed for real and imaginary  $\mu_1$ .

#### A. Transitions at zero and finite quark-number chemical potentials

First, we consider the case of  $\mu_q = 0$ . Figure 2 shows the  $T$  dependence of the order parameters  $\sigma$  and  $\Phi$ , while Fig. 3 represents chiral and Polyakov-loop susceptibilities,  $\chi_\sigma$  and  $\chi_\Phi$ , as a function of  $T$ , where the susceptibilities are normalized by  $T$  to become dimensionless [34, 53]. As shown in Fig. 2, the chiral and deconfinement transitions are crossover in both the PNJL and EPNJL models. Figure 3(a) presents  $\chi_\sigma$  and  $\chi_\Phi$  in the PNJL model. The peak position of  $\chi_\sigma$ , i.e., the critical temperature  $T_\sigma$  of the chiral transition, is much larger than the peak position of  $\chi_\Phi$ , that is, the critical temperature  $T_\Phi$  of the deconfinement transition. Figure 3(b) corresponds to  $\chi_\sigma$  and  $\chi_\Phi$  in the EPNJL model. In this model, the two transitions coincide with each other within numerical errors. Thus, the entanglement vertex  $G_s(\Phi)$  makes the correlation between the chiral restoration and the deconfinement transition stronger, as expected.

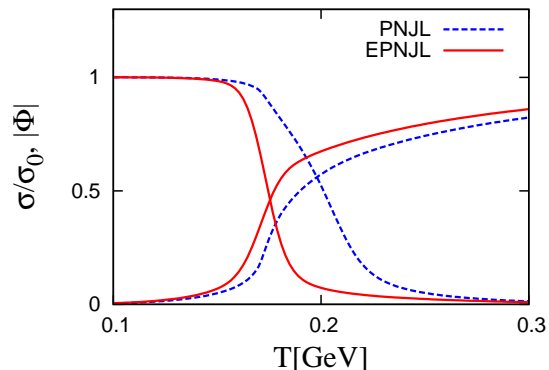


Fig. 2: (color online).  $T$  dependence of the chiral condensate and the Polyakov loop at  $\theta_q = 0$ . The curves that decrease (increase) as  $T$  increases represent the chiral condensate (Polyakov loop). The solid (dashed) curves are the results of the EPNJL (PNJL) model. Here, the chiral condensate is normalized by the value  $\sigma_0$  at  $T = 0$ .

Next, we consider the case of  $\theta_q = \pi/3$ . Figure 4 presents the  $T$  dependence of  $\sigma$  and the absolute value of  $\Phi$ . In the PNJL model, the deconfinement transition at  $T = 189$  MeV is first order, while the chiral transition is crossover;  $\sigma$  has a small jump at  $T = 189$  MeV, but it is just a discontinuity induced by the first-order deconfinement transition in  $|\Phi|$ . In the EPNJL model, the deconfinement transition at  $T = 185$  MeV seems to be very weak first-order, since  $|\Phi|$  has a small jump there within the present numerical accuracy, although it is not explicitly seen in Fig. 4.

Figure 5(a) shows that  $T_\sigma \gg T_\Phi$  in the PNJL model, while Fig. 5(b) shows that  $T_\sigma \approx T_\Phi$  in the EPNJL model. Thus, the

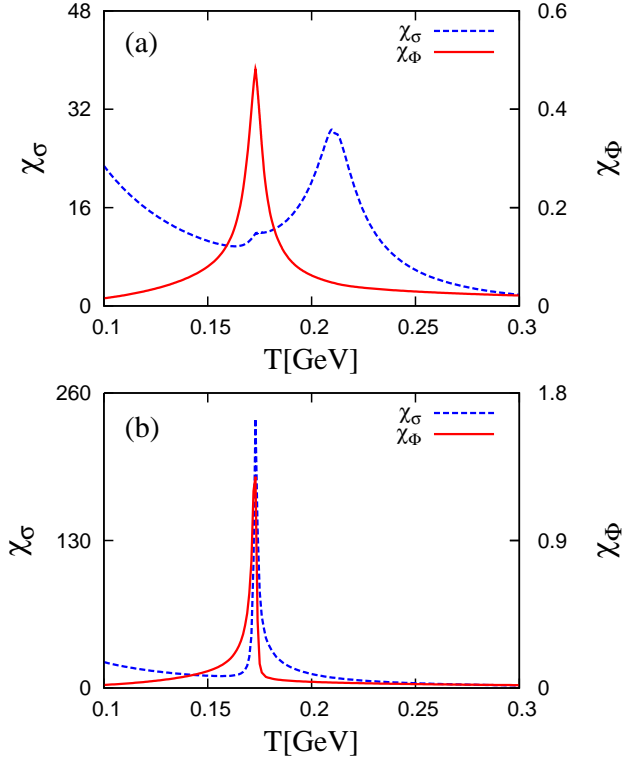


Fig. 3: (color online).  $T$  dependence of the susceptibilities of the chiral condensate (dashed curve) and the Polyakov loop (solid curve) at  $\theta_q = 0$ . Panels (a) and (b) correspond to the PNJL and EPNJL models, respectively.

entanglement vertex yields a stronger correlation between the chiral and deconfinement transitions also at  $\theta_q = \pi/3$ .

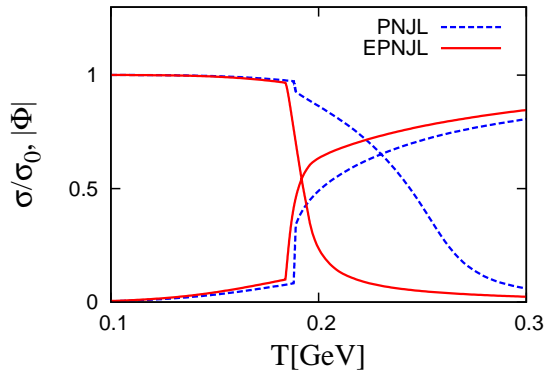


Fig. 4: (color online).  $T$  dependence of the chiral condensate and the Polyakov loop at  $\theta_q = \pi/3$ . The meaning of the curves is the same as in Fig. 2.

Figure 6 shows the phase diagram in the  $\theta_q$ - $T$  plane. In the original PNJL model,  $T_\sigma$  is much higher than  $T_\Phi$ , while both are close to each other in the EPNJL model. The vertical dot-dashed lines at  $\theta_q = \pi/3 \text{ mod } 2\pi/3$  are the RW transition line and the  $\mathbb{Z}_3$  images. The endpoint of the RW transition

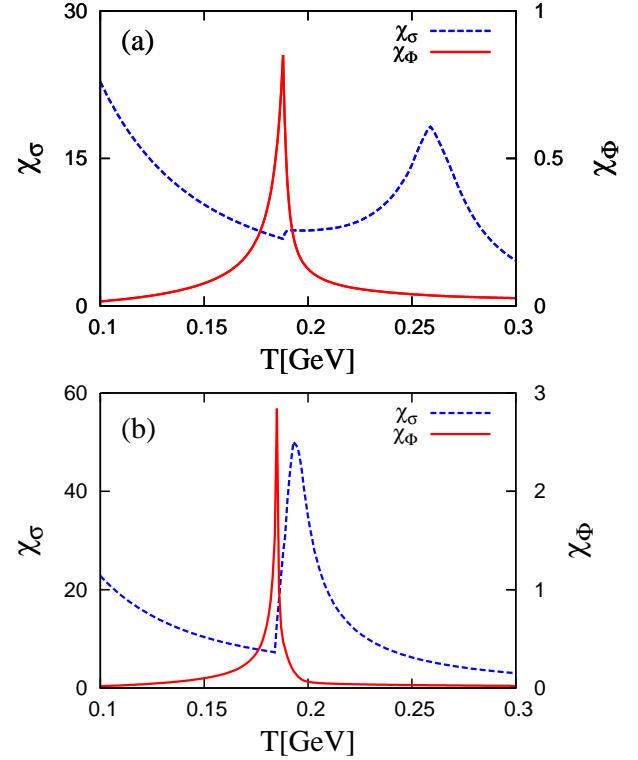


Fig. 5: (color online).  $T$  dependence of the susceptibilities of the chiral condensate (dashed curve) and the Polyakov loop (solid curve) at  $\theta_q = \pi/3$ . Panels (a) and (b) correspond to the results of the PNJL and EPNJL models, respectively.

line is located at  $T = T_E \approx 189$  MeV in the PNJL model and at 185 MeV in the EPNJL model. On the RW transition line at  $T > T_E$ ,  $C$  symmetry is spontaneously broken. As a consequence of this fact,  $\theta_q$ -odd quantities such as the phase  $\psi$  of the modified Polyakov loop  $\Psi$  are discontinuous, while  $\theta_q$ -even quantities have a cusp there [47–50]. Thus, the  $\theta_q$ -odd quantities are order parameters of the RW phase transition. In the original PNJL model, the transition is second order [50] for the Polyakov potential proposed by Fukushima [33], but first order [51, 52] for the Polyakov potential proposed by Rößner, Ratti and Weise [38]. The latter is more consistent with LQCD data at imaginary  $\mu_q$  than the former [51]. In the latter, the deconfinement phase transition is first order near the RW endpoint; the endpoint of the first-order deconfinement transition line is second order, and susceptibilities of several quantities diverge simultaneously there [51]. In the EPNJL model, such a first-order deconfinement transition line does not appear or very short if it does emerge, since the deconfinement transition at the RW endpoint seems to be a very weak first-order transition, as mentioned above.

Figure 7 shows results of the EPNJL model for the RW phase transition. Panel (a) presents the  $T$  dependence of the phase  $\psi$  of  $\Psi$  at  $\theta_q = \pi/3$  for the three cases  $m_0 = 5, 150,$  and  $400$  MeV. The RW transition at the endpoint is first order for  $m_0 = 5$  and  $400$  MeV, but second order for  $m_0 = 150$  MeV. In the limit of large  $m_0$ , the transition is obviously

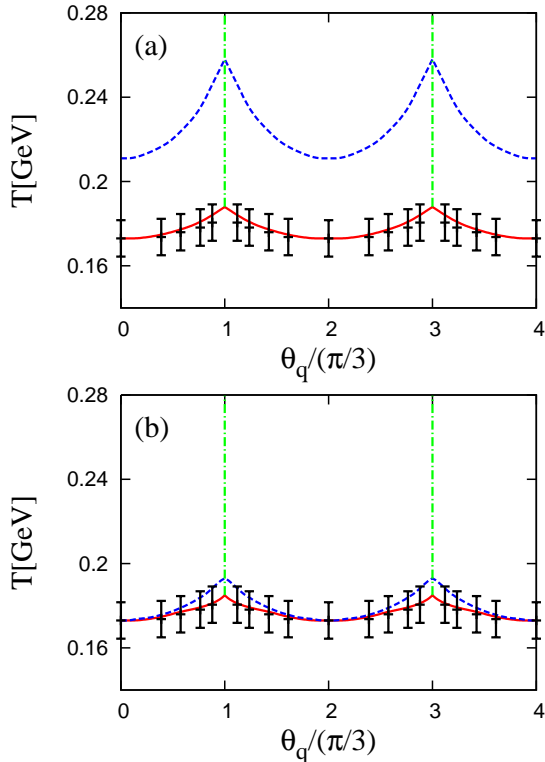


Fig. 6: (color online). Phase diagram in  $\theta_q$ - $T$  plane. Panel (a) is the result of the standard PNJL model with no entanglement vertex, while panel (b) is the result of the EPNJL model with  $(\alpha_1, \alpha_2) = (0.2, 0.2)$ . The solid (dashed) curves represent the deconfinement (chiral) transition. The vertical dot-dashed lines denote the RW transition lines. Lattice data are taken from Ref. [14].

first order, since the quark contribution to  $\Omega$  is suppressed and hence the deconfinement transition is controlled by the Polyakov potential  $\mathcal{U}$ . Meanwhile, the RW endpoint is always first order in the original PNJL model [51] and in the PNJL-8V model. Panel (b) shows the phase diagram of the RW phase transition in the  $m_0$ - $T$  plane; C symmetry is spontaneously broken above the curve, while it is preserved below the curve. The solid (dashed) curve shows that the RW phase transition is first (second) order on the boundary. The critical mass  $m_0(1 \rightarrow 2)$  [ $m_0(2 \rightarrow 1)$ ] from the first-order (second-order) to the second-order (first-order) transition is rather sensitive to the numerical accuracy. In the present numerical accuracy, the critical masses are  $m_0(1 \rightarrow 2) = 50 \pm 5$  MeV and  $m_0(2 \rightarrow 1) = 180 \pm 5$  MeV. This  $m_0$  dependence of the order of the RW endpoint is consistent with the recent result [19, 20] of LQCD.

Figure 8(a) shows the phase diagram in the whole  $\mu_q^2$ - $T$  plane obtained by the EPNJL model. The solid, dotted, dashed and dot-dashed curves represent the first-order chiral phase transition, the crossover chiral transition, the crossover deconfinement transition and the RW transition, respectively. The transition line (dashed and solid curves) in the region

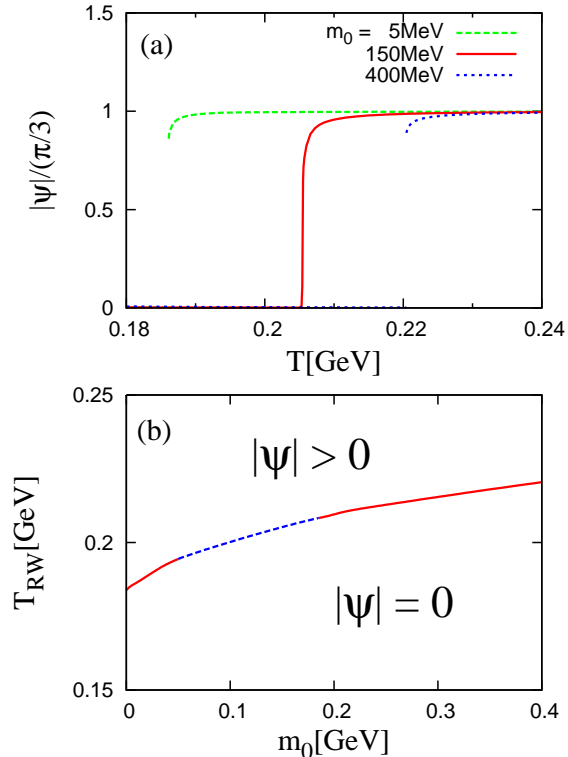


Fig. 7: (color online). The RW phase transition in the EPNJL model. In panel (a), the phase of the modified Polyakov loop at  $\theta_q = \pi/3$  is plotted as a function of  $T$  for three cases of light, intermediate, and heavy quark masses. Panel (b) shows the phase diagram of the RW phase transition in the  $m_0$ - $T$  plane. The solid (dotted) curve shows that the RW phase transition on the boundary is first (second) order.

$-0.0375 < \mu_q^2 < 0.08$  [GeV<sup>2</sup>] is expressed as

$$T = c_0 + c_1 \mu_q^2 + c_2 \mu_q^4, \quad (21)$$

where  $c_0 = 0.173$  [GeV],  $c_1 = -0.377$  [GeV<sup>-1</sup>], and  $c_2 = -2.71$  [GeV<sup>-3</sup>]. Point E is an endpoint of the RW transition, while point C is a CEP of the first-order chiral phase transition. Point A is a meeting point between the RW transition line and the crossover chiral transition line, while point B stands for the critical temperature of the chiral and deconfinement transitions at zero  $\mu_q$ . Locations of these points are tabulated in Table II. Thus, there exists a CEP not only in the PNJL-8V model [49] but also in the EPNJL model.

A	B	C	E
$(i\pi/3 \times 193, 193)$	$(0, 173)$	$(160, 161)$	$(i\pi/3 \times 185, 185)$

TABLE II: Locations  $(\mu_q, T)$  of points A, B, C and E. All locations are shown in MeV.

Figure 8(b) shows the first-order chiral phase transition line and its CEP in the original PNJL, the PNJL-8V, and the EPNJL models. The locations of the CEP in the three models are summarized in Table III. The CEP is located at smaller

$\mu_q$  and larger  $T$  in the EPNJL model compared with the other models. Thus, the entanglement vertex yields a drastic effect on the phase diagram at real  $\mu_q$ .

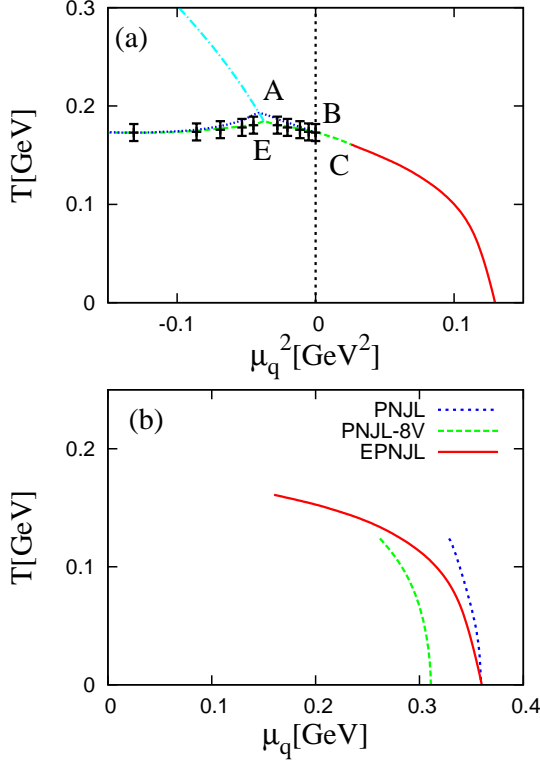


Fig. 8: (color online). (a) Phase diagram in the  $\mu_q^2$ - $T$  plane in the EPNJL model. The left (right) half-plane corresponds to imaginary (real)  $\mu_q$ . See the text for definitions of lines and points. Lattice data are taken from Ref. [14]. (b) The first-order chiral phase transition line and its CEP in the original PNJL, the PNJL-8V, and the EPNJL models.

PNJL	PNJL-8V	EPNJL
(327, 124)	(261, 124)	(160, 161)

TABLE III: Summary of locations  $(\mu_q, T)$  of CEP in three models. All locations are shown in MeV.

### B. Transitions at finite isospin chemical potential

The parameter set in the EPNJL model was determined in the previous subsection so as to reproduce LQCD data at zero and imaginary  $\mu_q$ . The validity of the parameter set is confirmed in this subsection for real and imaginary  $\mu_I$  where LQCD data are available.

The quark-number and isospin chemical potential,  $\mu_q$  and  $\mu_I$ , used in this paper are defined by

$$\mu_q = \frac{\mu_u + \mu_d}{2} = \frac{\mu_B}{3}, \quad \mu_I = \frac{\mu_u - \mu_d}{2} = \frac{\mu_{iso}}{2} \quad (22)$$

with the  $u$ -quark ( $d$ -quark) number chemical potential  $\mu_u$  ( $\mu_d$ ). Here,  $\mu_B$  and  $\mu_{iso}$  are the baryon and original isospin chemical potentials coupled, respectively, to the baryon charge  $\bar{B}$  and to the isospin charge  $\bar{I}_3$ . For comparison with LQCD, we use  $\mu_I$  as the isospin chemical potential instead of the original definition  $\mu_{iso}$ .

The formalism of the PNJL model at finite  $\mu_I$  is straightforward from Sec. II. The only essential difference is that the pseudoscalar condensate  $\pi \equiv \langle \bar{q}i\gamma_5\tau_1 q \rangle$  is nonzero, in general, at finite  $\mu_I$ . Therefore, the  $E^\pm(\mathbf{p})$  in (6) are replaced by

$$E_\pm^+(\mathbf{p}) = \sqrt{(E(\mathbf{p}) + \mu_I)^2 + N^2} \pm \mu_q \quad (23)$$

for the  $u$  quark and

$$E_\pm^-(\mathbf{p}) = \sqrt{(E(\mathbf{p}) - \mu_I)^2 + N^2} \pm \mu_q \quad (24)$$

for the  $d$  quark, where  $N = -2G_s(\Phi)\pi$ . The mesonic potential  $U_M$  is also changed into

$$U_M = G_s(\Phi)(\sigma^2 + \pi^2). \quad (25)$$

See Refs. [51] and [53] for the details of the formalism with finite  $\mu_I$ ; the only difference from the formalism is that  $G_s$  is replaced by  $G_s(\Phi)$  in the EPNJL model.

First, we consider imaginary  $\mu_I = i\theta_1 T$ . In Fig. 9, we show  $T$  dependence of  $\sigma$  and  $\Phi$  at  $\theta_1 = \pi/2$ . In the standard PNJL model with no entanglement vertex, the critical temperature  $T_\sigma$  of the crossover chiral transition is about twice the critical temperature  $T_\Phi$  of the first-order deconfinement transition. This weak entanglement between the chiral restoration and the deconfinement transition still persists in the PNJL-8V model also [51].

The origin of the weak entanglement is the following. The  $u$ -quark loop contribution to the  $T$ -dependent part of  $\Omega$  is nearly canceled by the  $d$ -quark loop contribution. Because of this cancellation, the thermal part  $\Omega^{\text{th}}$  of  $\Omega$  is reduced at  $\theta_1 = \pi/2$  and  $\mu_q = 0$  to

$$\begin{aligned} \Omega^{\text{th}} &= -4T \int \frac{d^3\mathbf{p}}{(2\pi)^3} \left\{ \text{Tr}_c \left[ \ln(1 + L e^{-\beta E(\mathbf{p}) - \frac{\pi}{2}i}) \right. \right. \\ &\quad \left. \left. + \ln(1 + L e^{-\beta E(\mathbf{p}) + \frac{\pi}{2}i}) \right] \right\} + \mathcal{U} \\ &= -4T \int \frac{d^3\mathbf{p}}{(2\pi)^3} \left\{ \text{Tr}_c \ln(1 + L^2 e^{-2\beta E(\mathbf{p})}) \right\} + \mathcal{U}, \end{aligned} \quad (26)$$

because  $L = L^\dagger$  at  $\mu_q = 0$ . In the last line of (26), the exponent in the first term is not  $\beta E(\mathbf{p})$  but  $2\beta E(\mathbf{p})$ , indicating that the temperature effect is reduced effectively by 1/2 in the first term. In the case of no entanglement vertex, the  $T$  dependence of  $\sigma$  is controlled by the first term, while that of  $\Phi$  is controlled by  $\mathcal{U}$ . Therefore,  $T_\sigma \approx 2T_\Phi$  in the original PNJL and the PNJL-8V model.

In the EPNJL model, the entanglement vertex appears not only in the first term of the last line of (26) but also in the vacuum part of  $\Omega$  [the first and the  $U_M$  terms in (6)]. This induces a strong correlation between the chiral restoration and

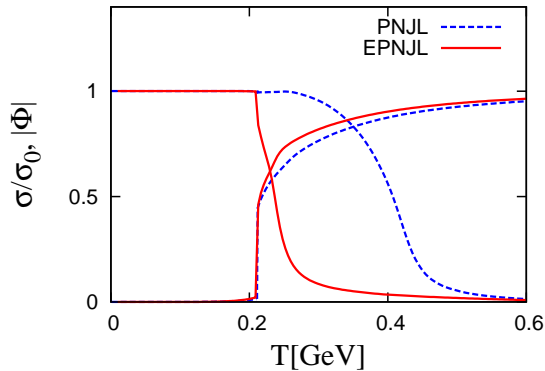


Fig. 9: (color online).  $T$  dependence of the chiral condensate and the Polyakov loop at  $\theta_1 = \pi/2$  and  $\mu_q = 0$ . See Fig. 2 for the meaning of lines.

the deconfinement transition. Actually, as shown by the solid curves in Fig. 9, both the transitions are first order and  $T_\sigma = T_\Phi$ . LQCD data at  $\theta_1 = \pi/2$  are not available in the two-flavor case but in the eight-flavor case [24]. The result of the EPNJL model is consistent with the LQCD result.

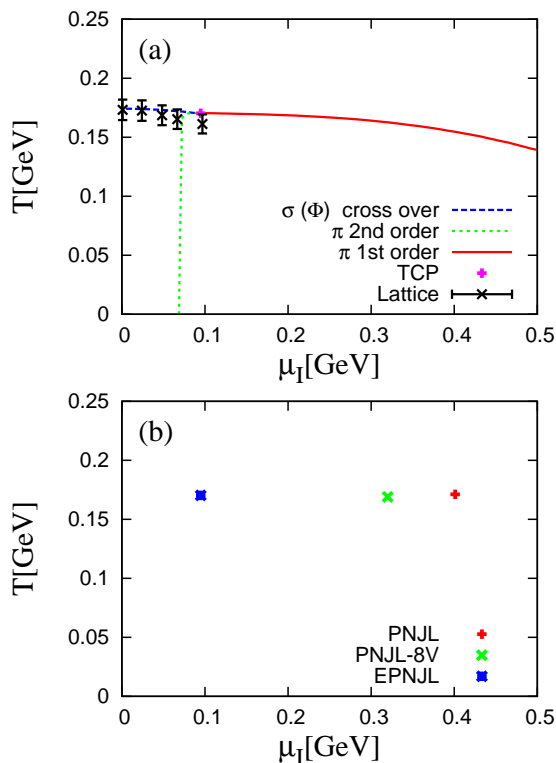


Fig. 10: (color online). (a) Phase diagram in the  $\mu_1$ - $T$  plane at  $\mu_q = 0$  in the EPNJL model. See the text for definitions of lines. LQCD data are taken from Ref. [23]. (b) The locations of the TCP at  $\mu_q = 0$  in the original PNJL, the PNJL-8V, and the EPNJL models.

Next, we consider real  $\mu_1$ . Figure 10(a) shows the phase diagram in the  $\mu_1$ - $T$  plane at  $\mu_q = 0$ . The solid and dotted lines

PNJL	PNJL-8V	EPNJL
(401,171)	(320,169)	(95,170)

TABLE IV: Summary of locations  $(\mu_1, T)$  of TCP at  $\mu_q = 0$  in three models. All locations are shown in MeV.

stand for the first-order and second-order pion-superfluidity transitions, respectively. The meeting point between the solid and dotted lines is a TCP by definition. The crossover chiral and deconfinement transitions agree with each other, as shown by the dashed line. The EPNJL result reproduces LQCD results on the chiral and deconfinement transitions and also on the pion-superfluidity transition. Figure 10(b) shows locations of the TCP at  $\mu_q = 0$  in the original PNJL, the PNJL-8V, and the EPNJL models. The entanglement vertex  $G_s(\Phi)$  largely affects the location of the TCP. The locations of the TCP in the three models are summarized in Table IV.

#### IV. SUMMARY

In summary, we have extended the PNJL model by introducing an entanglement vertex  $G_s(\Phi)$  phenomenologically. The effective vertex generates entanglement interactions between  $\sigma$  and  $\Phi$ . The EPNJL model with  $G_s(\Phi)$  can reproduce two phenomena simultaneously; one is the strong correlation between the chiral restoration and the deconfinement transition that appears in LQCD at imaginary  $\mu_q$  and real and imaginary  $\mu_1$ , and the other is the quark-mass dependence of the order of the RW endpoint predicted by LQCD very recently [19, 20]. Thus, the EPNJL model is consistent with all LQCD data at imaginary  $\mu_q$  and real and imaginary  $\mu_1$ .

The functional form of the entanglement vertex  $G_s(\Phi)$  is determined by respecting extended  $\mathbb{Z}_3$  symmetry, chiral symmetry and charge conjugation symmetry. The strength of the entanglement vertex is determined by LQCD data at imaginary  $\mu_q$ , and the validity of this model building is confirmed by LQCD data at real and imaginary  $\mu_1$ . The entanglement vertex largely changes the location of the TCP in the  $\mu_1$ - $T$  plane and the location of the CEP in the  $\mu_1$ - $T$  plane.

The present phenomenological approach seems to be complementary to the exact renormalization-group approach. It is highly expected that the functional form and the strength of the entanglement vertex will be determined in the future by the theoretical approach.

#### Acknowledgments

The authors thank P. de Forcrand, A. Nakamura, K. Fukushima, T. Saito and K. Kashiwa for useful discussions. H.K. also thanks M. Imachi, H. Yoneyama, H. Aoki and M. Tachibana for useful discussions. Y.S. is supported by JSPS Research Fellow.

- 
- [1] J. Cleymans, K. Redlich, H. Satz, and E. Suhonen, *Z. Phys. C-Particle and Fields* **33**, 151 (1986).
- [2] H. Kouno, and F. Takagi, *Z. Phys. C-Particle and Fields* **42**, 209 (1989).
- [3] L. McLerran, and R. D. Pisarski, *Nucl. Phys. A* **796**, 83 (2007).
- [4] Y. Hidaka, L. McLerran, and R. D. Pisarski, *Nucl. Phys. A* **808**, 117 (2008).
- [5] A. Barducci, R. Casalbuoni, G. Pettini, and R. Gatto, *Phys. Lett. B* **301**, 95 (1993).
- [6] K. Kashiwa, M. Yahiro, H. Kouno, M. Matsuzaki, and Y. Sakai, *J. Phys. G: Nucl. Part. Phys.* **36**, 105001 (2009).
- [7] M. Asakawa and K. Yazaki, *Nucl. Phys. A* **504**, 668 (1989).
- [8] H. Fujii, *Phys. Rev. D* **67**, 094018 (2003).
- [9] F. Karsch, and E. Laermann, *Phys. Rev. D* **50**, 6954 (1994); F. Karsch, *Lattice QCD at high temperature and density*, [hep-lat/0106019], *Lect. Notes Phys.* **583**, 209-249 (2002).
- [10] S. Aoki, M. Fukugita, S. Hashimoto, N. Ishizuka, Y. Iwasaki, K. Kanaya, Y. Kuramashi, H. Mino, M. Okawa, A. Ukawa, and T. Yoshie, *Phys. Rev. D* **57**, 3910 (1998).
- [11] Y. Aoki, Z. Fodor, S. D. Katz, and K. K. Szabo, *Phys. Lett. B* **643**, 46 (2006); Y. Aoki, S. Borsanyi, S. Durr, Z. Fodor, S. D. Katz, S. Krieg, and K. K. Szabo, *J. High Energy Phys.* **0906**, 088 (2009).
- [12] S. Borsanyi, Z. Fodor, C. Hoelbling, S. D. Katz, S. Krieg, C. Ratti, and K. K. Szabo, arXiv:1005.3508 [hep-lat] (2010).
- [13] J. B. Kogut and D. K. Sinclair *Phys. Rev. D* **77**, 114503 (2008).
- [14] P. de Forcrand and O. Philipsen, *Nucl. Phys. B* **642**, 290 (2002);
- [15] P. de Forcrand and O. Philipsen, *Nucl. Phys. B* **673**, 170 (2003).
- [16] M. D'Elia and M. P. Lombardo, *Phys. Rev. D* **67**, 014505 (2003); *Phys. Rev. D* **70**, 074509 (2004); M. D'Elia, F. D. Renzo, and M. P. Lombardo, *Phys. Rev. D* **76**, 114509 (2007);
- [17] H. S. Chen and X. Q. Luo, *Phys. Rev. D* **72**, 034504 (2005); arXiv:hep-lat/0702025 (2007).
- [18] L. K. Wu, X. Q. Luo, and H. S. Chen, *Phys. Rev. D* **76**, 034505 (2007).
- [19] M. D'Elia and F. Sanfilippo, *Phys. Rev. D* **80**, 111501 (2009).
- [20] P. de Forcrand and O. Philipsen, arXiv:1004.3144 [hep-lat](2010).
- [21] K. Nagata, A. Nakamura, Y. Nakagawa, S. Motoki, T. Saito and M. Hamada, arXiv:0911.4164 [hep-lat](2009).
- [22] T. Takaishi, P. de Forcrand and A. Nakamura, arXiv:1002.0890 [hep-lat](2010).
- [23] J. B. Kogut and D. K. Sinclair, *Phys. Rev. D* **70**, 094501 (2004).
- [24] P. Cea, L. Cosmai, M. D'Elia, C. Manneschi, and A. Papa, *Phys. Rev. D* **80**, 034501 (2009).
- [25] M. D'Elia and F. Sanfilippo, *Phys. Rev. D* **80**, 014502 (2009).
- [26] Y. Nambu and G. Jona-Lasinio, *Phys. Rev.* **122**, 345 (1961); *Phys. Rev.* **124**, 246 (1961).
- [27] S. P. Klevansky *Rev. Mod. Phys.* **64**, 649 (1992); T. Hatsuda and T. Kunihiro *Phys. Rep.* **247**, 221 (1994); M. Buballa *Phys. Rep.* **407**, 205 (2005).
- [28] M. Kitazawa, T. Koide, T. Kunihiro, and Y. Nemoto, *Prog. Theor. Phys.* **108**, 929 (2002).
- [29] A. A. Osipov, B. Hiller, and J. da Providência, *Phys. Lett. B* **634**, 48 (2006); A. A. Osipov, B. Hiller, J. Moreira, and A. H. Blin, *Eur. Phys. J. C* **46**, 225 (2006); A. A. Osipov, B. Hiller, J. Moreira, A. H. Blin, and J. da Providência, *Phys. Lett. B* **646**, 91 (2007); A. A. Osipov, B. Hiller, J. Moreira, and A. H. Blin, *Phys. Lett. B* **659**, 270 (2008); B. Hiller, A. A. Osipov, A. H. Blin, and J. da Providência, arXiv:hep-ph/0802.3193 (2008); B. Hiller, A. A. Osipov, J. Moreira, and A. H. Blin, arXiv:hep-ph/0809.2515 (2008); B. Hiller, J. Moreira, A. A. Osipov, and A. H. Blin, arXiv:hep-ph/0812.1532 (2008).
- [30] K. Kashiwa, H. Kouno, T. Sakaguchi, M. Matsuzaki, and M. Yahiro, *Phys. Lett. B* **647**, 446 (2007); K. Kashiwa, M. Matsuzaki, H. Kouno, and M. Yahiro, *Phys. Lett. B* **657**, 143 (2007).
- [31] P. N. Meisinger, and M. C. Ogilvie, *Phys. Lett. B* **379**, 163 (1996).
- [32] A. Dumitru, and R. D. Pisarski, *Phys. Rev. D* **66**, 096003 (2002); A. Dumitru, Y. Hatta, J. Lenaghan, K. Orginos, and R. D. Pisarski, *Phys. Rev. D* **70**, 034511 (2004); A. Dumitru, R. D. Pisarski, and D. Zschesche, *Phys. Rev. D* **72**, 065008 (2005).
- [33] K. Fukushima, *Phys. Lett. B* **591**, 277 (2004).
- [34] K. Fukushima, *Phys. Rev. D* **77**, 114028 (2008).
- [35] C. Ratti, M. A. Thaler, and W. Weise, *Phys. Rev. D* **73**, 014019 (2006); C. Ratti, S. Rößner, M. A. Thaler, and W. Weise, *Eur. Phys. J. C* **49**, 213 (2007).
- [36] S. K. Ghosh, T. K. Mukherjee, M. G. Mustafa, and R. Ray, *Phys. Rev. D* **73**, 114007 (2006).
- [37] E. Megías, E. R. Arriola, and L. L. Salcedo, *Phys. Rev. D* **74**, 065005 (2006).
- [38] S. Rößner, C. Ratti, and W. Weise, *Phys. Rev. D* **75**, 034007 (2007).
- [39] M. Ciminale, R. Gatto, N. D. Ippolito, G. Nardulli, and M. Ruggieri, *Phys. Rev. D* **77**, 054023 (2008); M. Ciminale, G. Nardulli, M. Ruggieri, and R. Gatto, *Phys. Lett. B* **657**, 64 (2007).
- [40] H. Hansen, W. M. Alberico, A. Beraudo, A. Molinari, M. Nardi, and C. Ratti, *Phys. Rev. D* **75**, 065004 (2007).
- [41] C. Sasaki, B. Friman, and K. Redlich, *Phys. Rev. D* **75**, 074013 (2007).
- [42] B. -J. Schaefer, J. M. Pawłowski, and J. Wambach, *Phys. Rev. D* **76**, 074023 (2007).
- [43] P. Costa, C. A. de Sousa, M. C. Ruivo, and H. Hansen, arXiv:hep-ph/0801.3616 (2008); P. Costa, M. C. Ruivo, C. A. de Sousa, H. Hansen, and W. M. Alberico, *Phys. Rev. D* **79**, 116003 (2009).
- [44] K. Kashiwa, H. Kouno, M. Matsuzaki, and M. Yahiro, *Phys. Lett. B* **662**, 26 (2008).
- [45] W. J. Fu, Z. Zhang, and Y. X. Liu, *Phys. Rev. D* **77**, 014006 (2008).
- [46] H. Abuki, M. Ciminale, R. Gatto, G. Nardulli, and M. Ruggieri, *Phys. Rev. D* **77**, 074018 (2008); H. Abuki, M. Ciminale, R. Gatto, N. D. Ippolito, G. Nardulli, and M. Ruggieri, *Phys. Rev. D* **78**, 014002 (2008); H. Abuki, R. Anglani, R. Gatto, G. Nardulli, and M. Ruggieri, *Phys. Rev. D* **78**, 034034 (2008).
- [47] Y. Sakai, K. Kashiwa, H. Kouno, and M. Yahiro, *Phys. Rev. D* **77**, 051901(R) (2008); *Phys. Rev. D* **78**, 036001 (2008); K. Kashiwa, M. Matsuzaki, H. Kouno, Y. Sakai, and M. Yahiro, *Phys. Rev. D* **79**, 076008 (2009); K. Kashiwa, H. Kouno, and M. Yahiro, *Phys. Rev. D* **80**, 117901 (2009);
- [48] Y. Sakai, K. Kashiwa, H. Kouno, M. Matsuzaki, and M. Yahiro, *Phys. Rev. D* **78**, 076007 (2008).
- [49] Y. Sakai, K. Kashiwa, H. Kouno, M. Matsuzaki, and M. Yahiro, *Phys. Rev. D* **79**, 096001 (2009);
- [50] H. Kouno, Y. Sakai, K. Kashiwa, and M. Yahiro, *J. Phys. G: Nucl. Part. Phys.* **36**, 115010 (2009).
- [51] Y. Sakai, H. Kouno, and M. Yahiro, *J. Phys. G: Nucl. Part. Phys.* **37**, 105007 (2010).

- [52] T. Matsumoto, K. Kashiwa, H. Kouno, K. Oda, and M. Yahiro, arXiv:hep-ph/1004.0592 [hep-ph] (2010).
- [53] T. Sasaki, Y. Sakai, H. Kouno, and M. Yahiro, arXiv:hep-ph/1005.0910 [hep-ph] (2010).
- [54] Y. Sakai, T. Sasaki, H. Kouno, and M. Yahiro, arXiv: 1005.0993 [hep-ph](2010).
- [55] A. Roberge and N. Weiss, Nucl. Phys. **B275**, 734 (1986).
- [56] J. Braun, L. M. Haas, F. Marhauser, and J. M. Pawłowski, arXiv:0908.0008 [hep-ph] (2009).
- [57] K.-I. Kondo, arXiv:1005.0314 [hep-th] (2010).
- [58] C. Wetterich, Phys. Lett. B **301**, 90 (1991).
- [59] G. Boyd, J. Engels, F. Karsch, E. Laermann, C. Legeland, M. Lütgemeier, and B. Petersson, Nucl. Phys. **B469**, 419 (1996).
- [60] O. Kaczmarek, F. Karsch, P. Petreczky, and F. Zantow, Phys. Lett. B **543**, 41 (2002).
- [61] F. Karsch, E. Laermann, and A. Peikert, Nucl. Phys. B **605**, 579 (2002).
- [62] M. Kaczmarek and F. Zantow, Phys. Rev. D **71**, 114510 (2005);